

CoFi-Dec: Hallucination-Resistant Decoding via Coarse-to-Fine Generative Feedback in Large Vision-Language Models

Zongsheng Cao*
agiczs@gmail.com
Researcher

Jun Xie
xiejun@lenovo.com
PCIE

Yangfan He*
he00577@umn.edu
UMN

Feng Chen
chenfeng@lenovo.com
PCIE

Anran Liu*†
anniegogo1008@gmail.com
Researcher

Zepeng Wang†
wangzpb@lenovo.com
PCIE

Abstract

Large Vision-Language Models (LVLMs) have achieved impressive progress in multi-modal understanding and generation. However, they still tend to produce hallucinated content that is inconsistent with the visual input, which limits their reliability in real-world applications. We propose **CoFi-Dec**, a training-free decoding framework that mitigates hallucinations by integrating generative self-feedback with coarse-to-fine visual conditioning. Inspired by the human visual process from global scene perception to detailed inspection, CoFi-Dec first generates two intermediate textual responses conditioned on coarse- and fine-grained views of the original image. These responses are then transformed into synthetic images using a text-to-image model, forming multi-level visual hypotheses that enrich grounding cues. To unify the predictions from these multiple visual conditions, we introduce a Wasserstein-based fusion mechanism that aligns their predictive distributions into a geometrically consistent decoding trajectory. This principled fusion reconciles high-level semantic consistency with fine-grained visual grounding, leading to more robust and faithful outputs. Extensive experiments on six hallucination-focused benchmarks show that CoFi-Dec substantially reduces both entity-level and semantic-level hallucinations, outperforming existing decoding strategies. The framework is model-agnostic, requires no additional training, and can be seamlessly applied to a wide range of LVLMs. The implementation is available at <https://github.com/AI-Researcher-Team/CoFi-Dec>.

CCS Concepts

• Computing methodologies → Natural language processing.

Keywords

Mitigating Hallucinations, Large Vision-Language Models

*Equal contribution

†Corresponding author

Permission to make digital or hard copies of all or part of this work for personal or classroom use is granted without fee provided that copies are not made or distributed for profit or commercial advantage and that copies bear this notice and the full citation on the first page. Copyrights for components of this work owned by others than the author(s) must be honored. Abstracting with credit is permitted. To copy otherwise, or republish, to post on servers or to redistribute to lists, requires prior specific permission and/or a fee. Request permissions from permissions@acm.org.

MM'25, October 27–31, 2025, Dublin, Ireland

© 2025 Copyright held by the owner/author(s). Publication rights licensed to ACM.

ACM ISBN 979-8-4007-2035-2/2025/10

<https://doi.org/10.1145/3746027.3754791>

ACM Reference Format:

Zongsheng Cao, Yangfan He, Anran Liu, Jun Xie, Feng Chen, and Zepeng Wang. 2025. CoFi-Dec: Hallucination-Resistant Decoding via Coarse-to-Fine Generative Feedback in Large Vision-Language Models. In *Proceedings of the 33th ACM International Conference on Multimedia (MM '25), October 27–31, 2025, Dublin, Ireland*. ACM, New York, NY, USA, 15 pages. <https://doi.org/10.1145/3746027.3754791>

1 Introduction

In recent years, large vision-language models (LVLMs) have attracted extensive attention, and achieved impressive results across a range of multimodal tasks, including image captioning and visual question answering, by extending the representational power of Large Language Models (LLMs) to process visual data [2, 51]. Despite their success in jointly modeling visual and textual information, LVLMs remain prone to generating hallucinations: outputs that contradict or deviate from the actual visual input. [18, 30, 49, 52]. Such behavior poses serious risks of misinformation, undermining the trustworthiness of these models and limiting their applicability in safety-critical or real-world scenarios [3, 34, 58].

A growing body of work attributes this issue to the models' tendency to overfit to language priors, a byproduct of imbalanced training data that leads them to prioritize linguistic patterns over grounded visual evidence [3, 26, 34]. To address this, several methods have focused on hallucination suppression through additional supervision or enhanced training schemes [5, 30, 57]. While these approaches have shown effectiveness, their dependence on extensive retraining and additional annotated data significantly limits their scalability and usability in downstream applications.

To overcome these limitations, a newer class of approaches shifts focus from training-time interventions to decoding-time strategies [13, 20, 25]. In particular, recent advances in contrastive decoding, achieved without any model retraining, have shown promising results in reducing hallucinations [29]. These methods work by contrasting token predictions conditioned on faithful visual input against those generated under intentionally biased or weakened conditions, such as missing or corrupted images [14, 26], noisy prompts [46], or truncated intermediate layers [10]. This inference-time strategy provides an efficient and generalizable pathway to mitigate hallucinations without incurring the overhead of additional training. Moreover, some prior work has explored hallucination mitigation through either architectural modifications [28, 33, 44], fine-tuning with annotated data, or post-hoc filtering. More recently, decoding-time strategies have attracted increasing attention due to their training-free and model-agnostic properties. Among

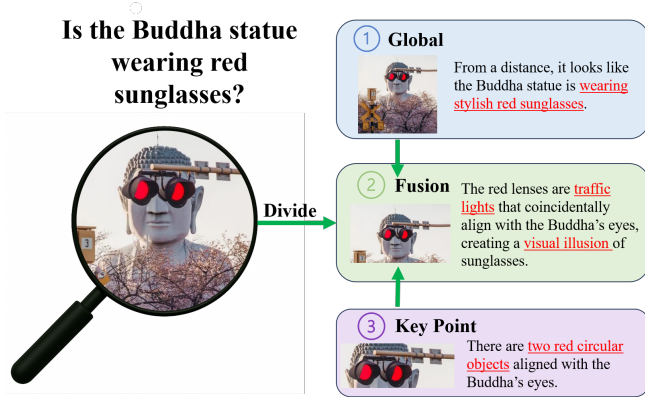


Figure 1: The illustration of the importance of combining coarse-grained and fine-grained visual information to avoid misleading global interpretations. By decomposing the scene, we uncover that the perceived red sunglasses are actually traffic lights, highlighting the need for multi-scale reasoning in visual understanding.

these, feedback-based decoding methods attempt to revise or verify model predictions by incorporating auxiliary signals, such as retrieved factual knowledge or images synthesized from textual hypotheses.

While conceptually promising, these approaches are often limited in three critical aspects. As shown in Fig.1. First, most feedback-based methods rely solely on the original image input and operate at a single resolution, overlooking the inherent multiscale structure of visual information. As a result, they may fail to detect inconsistencies that manifest at different semantic levels, such as global layout versus object details. Second, generative feedback is typically used in a post-hoc fashion, serving merely as a reference for re-ranking or answer replacement. This weakens its influence on the actual token-level generation process. Third, existing strategies rarely incorporate feedback in a fine-grained, step-by-step manner that allows cumulative correction and refinement during decoding.

In this work, we propose **CoFi-Dec**, a new decoding framework that addresses these limitations through *coarse-to-fine guided generative feedback*. Our key insight stems from the observation that hallucinations often result from imbalanced attention across visual granularities. To address this, we design a human-inspired decoding process that mimics perceptual strategies in visual cognition, where coarse scanning precedes focused inspection. Motivated by previous work [35, 56], given an input image, CoFi-Dec first constructs two visual pathways by decomposing the image into coarse-grained and fine-grained representations. The coarse view captures global context by uniformly downsampling the image into low-resolution patches, while the fine view highlights local semantics through high-resolution crops around salient or ambiguous regions. These two complementary inputs are used to generate independent textual responses using an LVLM. Each response serves as a semantic hypothesis derived from a different perceptual lens. To convert these hypotheses into actionable feedback, we employ a generative vision model (e.g., Stable Diffusion) to synthesize two pseudo-images

corresponding to the coarse- and fine-grained responses. These generated images serve as the model’s self-imagined reflections of its own beliefs, capturing what the model “sees” at different levels of abstraction. Rather than treating these synthetic images as auxiliary evidence, we integrate them along with the original image into the decoding loop. This integration guides subsequent token generation.

At each decoding step, CoFi-Dec computes three conditional token distributions, each based on a distinct visual condition: the original image, the synthesized coarse image, and the synthesized fine image. These distributions are then fused using a *Wasserstein barycenter optimization*, which computes a geometry-aware consensus across the semantic token space. Unlike naïve averaging, this method respects the underlying structure of the vocabulary space and encourages smooth, semantically meaningful corrections.

This multi-path decoding design allows CoFi-Dec to cross-reference visual semantics at multiple scales, verify generated content from self-imagined feedback, and continuously refine output in a self-correcting fashion. Importantly, the entire framework is training-free, modular, and compatible with a wide range of pre-trained LVLMs, making it practical for real-world deployment.

To summarize, our main contributions are:

- We propose **CoFi-Dec**, a novel training-free decoding framework that incorporates coarse-to-fine generative visual feedback to mitigate hallucinations in LVLMs.
- We design a multi-granular visual decomposition mechanism that mirrors human-like inspection patterns, enabling distinct semantic views for generative self-verification.
- We introduce a Wasserstein-based fusion strategy that jointly considers original and feedback-conditioned predictions to produce geometrically consistent token-level decoding.
- We conduct extensive experiments across six hallucination-sensitive benchmarks, demonstrating that CoFi-Dec consistently outperforms state-of-the-art decoding baselines in hallucination mitigation.

2 Related Work

Hallucination in LVLMs. Autoregressive large language models such as LLaMA 2 [45], PaLM 2 [9], and Vicuna [8] have catalysed a rapid shift from text-only modelling to large vision-language models (LVLMs) [2, 12, 33, 51]. In a typical LVLM, raw image features are passed through a lightweight adapter or projection layer, allowing pixel-level signals to share a common embedding space with tokens; this simple alignment lets a single backbone reason fluidly across modalities and has driven state-of-the-art results on image captioning, visual question answering, and allied benchmarks [3, 34].

Performance gains, however, mask a persistent liability, which is called hallucination. LVLMs still invent objects, attributes, or relations that are absent from the scene [3, 30, 34]. Current mitigation strategies fall into three broad camps. Alignment methods (e.g. RLHF) try to steer generation toward fidelity [18, 43]. Training-time regularisers embed auxiliary losses that penalise visual-textual mismatch [7, 21]. Data-centric approaches toughen the model with noise or adversarial samples [31, 54]. A complementary, post-hoc line edits outputs via verifier–editor cascades [52, 59]. While all

show promise, they typically demand heavy curation or repeated fine-tuning, which hampers scalability and real-world adoption.

A growing body of work now targets training-free, zero-tuning add-ons that enhance pretrained LVLMs without touching their weights. Two main families have emerged. Contrastive-decoding schemes [14, 26] suppress hallucinations by ranking or subtracting continuations produced under different sampling rules, whereas guided-decoding techniques [6, 13, 48] inject auxiliary signals directly into the token-generation loop. Most recently, Zhang et al. [56] extends this trend: they create synthetic images as iterative “visual critiques,” allowing the model to refine its own drafts and curb hallucinations in a manner reminiscent of human double-checking. **Text-to-Image Synthesis.** Text-to-image synthesis seeks to translate a free-form sentence into a picture that is both semantically faithful and visually convincing [16, 60]. Breakthroughs in deep generative modelling [17, 55] have propelled the field forward, producing three flagship families: diffusion models [19, 24, 36, 39, 40], generative adversarial networks (GANs) [23, 41], and autoregressive token predictors [4, 53]. Diffusion methods now dominate thanks to their ability to render highly detailed, photorealistic imagery while offering precise user control [11, 50]. When exposed to web-scale corpora such as LAION [42], they learn tight text–image correspondences that translate into strong zero-shot performance on downstream tasks, from image classification [27] to semantic segmentation [1, 47].

Recent work by Jiao et al. [22] shows that diffusion generators can improve fine-grained recognition. Using Stable Diffusion XL [37], they built the Img-Diff corpus, which contains paired images with subtle variations, and demonstrated that fine-tuning LVLMs on this synthetic set increases accuracy on multiple VQA benchmarks. In contrast to such data-augmentation-and-retraining pipelines, Zhang et al. [56] takes a training-free approach. During inference, a pretrained diffusion model acts as a visual feedback loop: it converts the LVLM’s initial text into synthetic images and feeds them back to the model for self-correction. This iterative process improves factual consistency and visual grounding while keeping the original LVLM weights unchanged, thus maintaining its deployment footprint. However, figures often contain both coarse-grained and fine-grained features, which previous work has overlooked. Addressing these features remains an open challenge for hallucination resistance.

3 Methodology

In this paper, we introduce **CoFi-Dec**, a novel training-free framework designed to enhance the reliability of LVLM responses through recursive refinement using feedback from a text-to-image generative model, as depicted in Figure 2.

Problem Setting. We assume access to a vision-language model (LVLM) parameterized by θ , which receives a visual input v and a textual query \mathbf{x} , and aims to generate a coherent and relevant textual response sequence \mathbf{y} in an autoregressive fashion. The image v is first encoded by a vision encoder and subsequently mapped into a sequence of visual tokens via a vision-language projection module, such as a Q-Former [28] or a linear projection layer [33], which aligns the visual features with the language model’s embedding space. These visual tokens, together with the tokenized textual query, are fed into the language encoder to condition the generative

process. Formally, the generation at each time step t is governed by the following distribution:

$$y_t \sim p_\theta(y_t | v, \mathbf{x}, \mathbf{y}_{<t}) \propto \exp f_\theta(y_t | v, \mathbf{x}, \mathbf{y}_{<t}), \quad (1)$$

where y_t denotes the token generated at step t , and $\mathbf{y}_{<t} = [y_0, \dots, y_{t-1}]$ represents the sequence of previously generated tokens. The function f_θ outputs the unnormalized logit scores over the vocabulary \mathcal{V} , which are then transformed into probabilities for sampling. This autoregressive decoding continues until an end-of-sequence token is generated, yielding the final response $\mathbf{y} = [y_0, \dots, y_T]$.

3.1 Generative Feedback with Multi-Granular Conditioning

Despite recent advances, hallucination remains a persistent challenge for Large Vision-Language Models (LVLMs), especially in scenarios requiring precise grounding of visual entities. Existing decoding strategies, leverage auxiliary synthetic visual signals to refine the output, yet they predominantly rely on the original single-scale image input. Such representations may fail to capture critical visual nuances that are essential for resolving ambiguity or verifying semantic consistency.

Motivated by the multi-scale processing mechanism in human vision, where observers first perform a coarse scan of the visual field before engaging in fine-detail scrutiny, we propose a novel decoding framework that jointly incorporates coarse-grained, fine-grained, and original visual cues. By structuring the visual input into a hierarchical multi-resolution context and integrating it into a generative feedback loop, our model achieves higher robustness and fidelity in grounding visual content during generation.

Hierarchical Visual Decomposition. Given an input image $I_0 \in \mathbb{R}^{H \times W \times 3}$ and an associated textual prompt T , we first decompose the image into two complementary sets of patches that capture different granularity levels:

- **Coarse-grained views** $\mathcal{I}_c = \{I_c^1, \dots, I_c^n\}$: Each I_c^i is obtained by uniformly dividing I_0 into n non-overlapping low-resolution patches, preserving the global spatial structure while discarding fine details. This resembles a downsampled global scan that preserves contextual semantics.
- **Fine-grained views** $\mathcal{I}_f = \{I_f^1, \dots, I_f^m\}$: Each I_f^j is a high-resolution crop focusing on salient or uncertain regions, derived from either learned attention maps or region proposal algorithms. These patches highlight local discriminative features that are potentially omitted by coarse processing.

In this way, the full multi-resolution visual input is denoted by the unified set:

$$\mathcal{I} = I_0 \cup \mathcal{I}_c \cup \mathcal{I}_f. \quad (2)$$

To this end, the initial response R_0 is generated by an LVLM conditioned only on the original image I_0 and the prompt T :

$$R_0 = \text{LVLM}(I_0, T). \quad (3)$$

We then perform two conditional generations under different granularity contexts from coarse- and fine-grained perspectives:

$$R_c = \text{LVLM}(\mathcal{I}_c, T), \quad (4)$$

$$R_f = \text{LVLM}(\mathcal{I}_f, T). \quad (5)$$

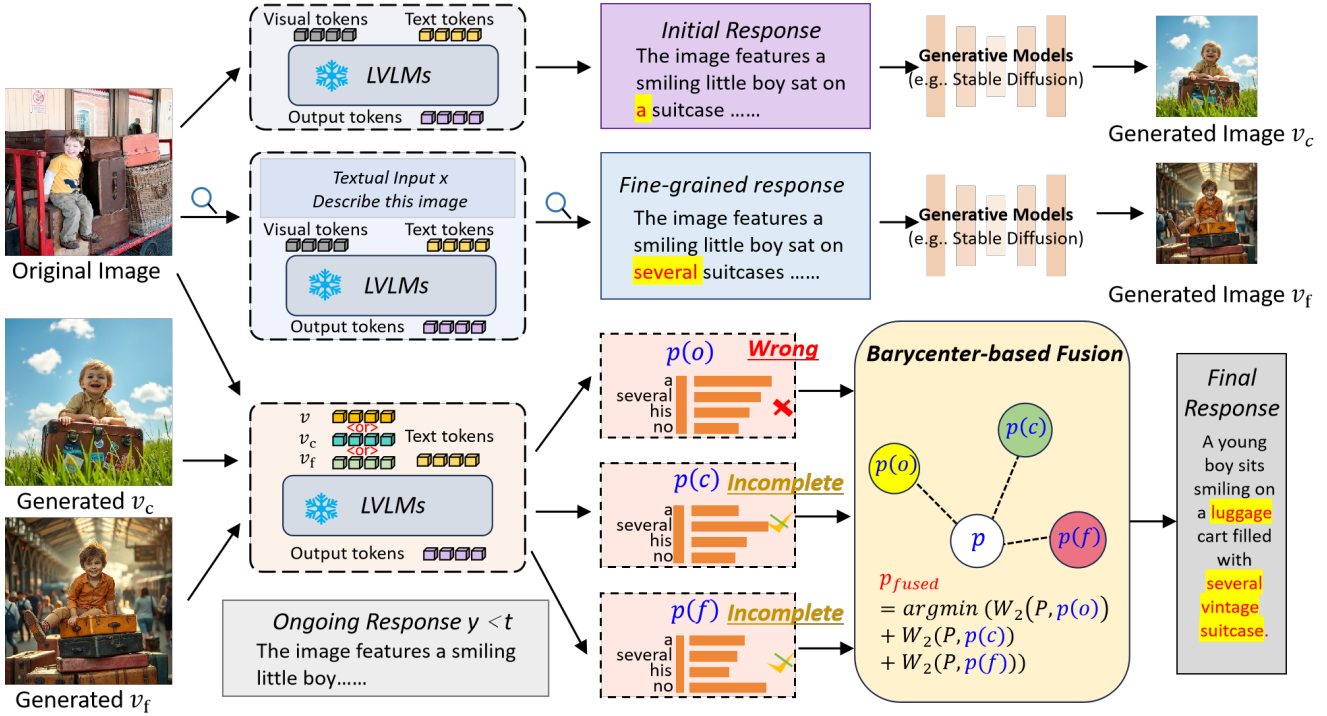


Figure 2: Overview of our proposed CoFi-Dec. Our method follows a coarse-to-fine generative feedback framework to enhance the fidelity of image-grounded text generation. By generating both coarse- and fine-grained textual descriptions from the original image and synthesizing corresponding images, we obtain multi-perspective visual feedback. These signals are then fused using a Wasserstein barycenter to produce a final response that is semantically rich, visually grounded, and resistant to hallucination.

To enable self-verification, a generative vision model G (e.g., Stable Diffusion) is used to synthesize a pseudo-image based on the textual hypothesis. The synthesized image serves as a reflection of the model’s internal belief and facilitates visual grounding in subsequent refinement stages. We obtain the corresponding synthesized figures v_c and v_f as follows:

$$v_c = G(R_c), v_f = G(R_f). \quad (6)$$

3.2 Self-Correcting Decoding with Generative Feedback

In this part, we describe how to incorporate the complementary cues from coarse-grained, fine-grained, and original image views into the decoding process in a more fine-grained and dynamic manner. While previous sections focus on generating separate responses conditioned on different visual granularities, these responses are inherently static and limited in their ability to reconcile semantic discrepancies across views. To address this, we move beyond fixed-level conditioning and explore a decoding-time integration strategy that operates at the token level. Our goal is to enable more precise alignment between multimodal inputs and language outputs by leveraging the unique strengths of each visual perspective: the original image captures layout and raw semantics, the coarse-grained view emphasizes holistic structure, and the fine-grained view provides object-level precision.

Specifically, rather than relying on isolated end-to-end responses from each visual condition, we propose a *self-correcting decoding* strategy that dynamically fuses the predictive signals across granularities for each generated token. This allows the model to adaptively weigh global context, structural composition, and localized evidence in a principled way at every step of generation, thus enabling more faithful and grounded outputs.

Let v , v_c , and v_f denote the visual embeddings extracted from the original image, the synthesized coarse-grained context, and the fine-grained visual reference, respectively. For a given prompt \mathbf{x} and previously generated sequence $\mathbf{y}_{<t}$, the model produces three conditional probability distributions over the vocabulary for the next token y_t :

$$\begin{aligned} p_\theta(y_t|v, \mathbf{x}, \mathbf{y}_{<t}) &= \text{Softmax}[f_\theta(y_t|v, \mathbf{x}, \mathbf{y}_{<t})], \\ p_\theta(y_t|v_c, \mathbf{x}, \mathbf{y}_{<t}) &= \text{Softmax}[f_\theta(y_t|v_c, \mathbf{x}, \mathbf{y}_{<t})], \\ p_\theta(y_t|v_f, \mathbf{x}, \mathbf{y}_{<t}) &= \text{Softmax}[f_\theta(y_t|v_f, \mathbf{x}, \mathbf{y}_{<t})]. \end{aligned} \quad (7)$$

To obtain a unified prediction distribution that effectively integrates multi-granular visual information, we leverage the concept of Wasserstein barycenters to fuse the token-level output distributions conditioned on the original image v , the coarse-grained reference v_c , and the fine-grained reference v_f . Unlike simple averaging or heuristic weighting schemes, the Wasserstein barycenter provides a principled way to compute a central distribution that

minimizes the overall transportation cost with respect to the constituent distributions, thereby preserving the underlying semantic geometry of the token space.

Formally, for a fixed decoding timestep t , we denote the three predictive distributions over the vocabulary as $P_t^{(v)} = p_\theta(y_t|v, \mathbf{x}, \mathbf{y}_{<t})$, $P_t^{(c)} = p_\theta(y_t|v_c, \mathbf{x}, \mathbf{y}_{<t})$, and $P_t^{(f)} = p_\theta(y_t|v_f, \mathbf{x}, \mathbf{y}_{<t})$, each represented as a probability vector in the $|\mathcal{V}|$ -dimensional simplex, where \mathcal{V} is the vocabulary.

To compute the fused distribution $P_t^{(\text{fused})}$ that serves as the final prediction for y_t , we solve the following optimization problem:

$$P_t^{(\text{fused})} = \arg \min_{P \in \Delta^{|\mathcal{V}|}} \left(W(P, P_t^{(v)}) + W(P, P_t^{(c)}) + W(P, P_t^{(f)}) \right), \quad (8)$$

where $W(P, Q)$ denotes the Wasserstein distance between two distributions P and Q . This formulation ensures that the fused distribution is not only probabilistically valid but also geometrically faithful to the structure of the input distributions.

Once the barycenter $P_t^{(\text{fused})}$ is computed for each timestep t , it is used in place of the individual conditional distributions for token selection during generation. Notably, this fusion mechanism allows the model to adaptively reconcile the high-level contextual cues from v_c with the fine-grained semantic alignment from v_f , grounded by the original image v , yielding a robust and geometrically consistent prediction. This Wasserstein-based fusion strategy thus constitutes a key component of our model's capability to perform multi-granular visual reasoning during language generation.

Remark 3.1. Our proposed framework introduces a unified decoding paradigm that explicitly models multi-resolution visual reasoning and aligns it with generative feedback. Compared to prior work that treats feedback as a post-hoc correction, we integrate it into a multi-path decoding framework where each visual granularity serves as an independent yet complementary source of evidence. By mirroring human-like inspection patterns, in which a global preview is followed by selective zoom-in, the model acquires a more holistic and reliable understanding of the visual scene. This reduces reliance on spurious correlations and encourages grounded generation, especially in scenarios with ambiguous, cluttered, or fine-detailed imagery.

4 Experiments

In this section, we evaluate our model through a suite of benchmark trials designed to gauge its ability to suppress hallucinations in LVLMs, and we juxtapose the resulting metrics with those reported by the strongest contemporary baselines.

4.1 Experimental Settings

LVLMs. To evaluate our model, we ran a comprehensive test suite on three headline open-source LVLMs: the upgraded **LLaVA-1.5** [32], **InstructBLIP** [12], and Alibaba's **Qwen-VL** [2]. The first two share an identical textual backbone, *Vicuna-7B* [8], itself a dialogue-oriented adaptation of *LLaMA* [45]. By contrast, Qwen-VL is anchored in the 7-billion-parameter Qwen family. For our own trials, we simply plug the proposed CoFi-Dec module into the publicly released *Qwen-VL-Chat* checkpoint, leaving all original weights intact.

Benchmarks. Following previous work [20, 56], our empirical study taps into six publicly available testbeds that jointly probe a model's resistance to hallucination and its overall visual-reasoning prowess: (1) **POPE** [30] focuses on object hallucination by presenting binary questions that test whether the model can correctly identify the presence or absence of objects in an image. (2) **CHAIR** [38] examines hallucinations in free-form image captions, requiring models to describe images randomly sampled from the MSCOCO validation set, with attention to visual grounding. (3) **MME-Hallucination** [15] provides a fine-grained evaluation of both object-level and attribute-level hallucinations via four sub-tasks: *existence*, *count*, *position*, and *color*. (4) **MMBench** [35] serves as a broad-spectrum evaluation suite, covering 20 aspects of multimodal reasoning to test LVLMs' general understanding capabilities. (5) **MMVP** [44] targets fine-grained recognition through CLIP-blind image pairs, challenging models with binary questions across 150 curated examples. (6) **LLaVA-Bench** comprises 24 images ranging from complex real-world scenes to artistic renderings (e.g., memes, paintings, and sketches), paired with 60 intricate questions designed to test both visual perception and contextual comprehension.

Baselines. We begin with a straightforward baseline in which decoding is performed in the conventional manner, that is, each token is sampled directly from the softmax-normalized output probabilities. Beyond this, we evaluate our approach against three state-of-the-art decoding strategies: VCD [26], M3ID [14], and RITUAL [48]. For benchmarks such as CHAIR [38] and MME-Hallucination [15], we expand the comparison set to include additional recent methods, namely Woodpecker [6], HALC [6], DoLa [10], OPERA [20], and DeGF [56]. Performance results for these baselines are derived from our own re-implementation based on their officially released source code.

Implementation Details. In all experiments, we maintain consistency with the standard input formatting adopted by LLaVA-1.5 [32] and InstructBLIP [12]. To account for variability, we run each MME benchmark experiment three times with different random seeds and report both the mean accuracy and standard deviation.

4.2 Results and Discussions

Results on POPE. Table 1 presents a comparative analysis of our proposed method and several strong baselines on the POPE benchmark, evaluated under three distinct negative sampling strategies across three different datasets. More details can refer to Appendix. Our approach consistently yields superior performance over all competitors across the 18 evaluation settings, achieving the highest accuracy, precision, and F1 score on both LVLM architectures. Specifically, we observe significant gains in different metrics when compared to the next-best method. These results indicate that integrating a generative reference allows the model to better capture fine-grained visual cues, effectively mitigating object hallucinations. Additionally, while many decoding approaches exhibit overconfidence and often default to affirmative answers, our self-refining decoding strategy demonstrates a more cautious response pattern. This is reflected in its consistently higher precision, indicating a stronger ability to avoid false positives and resist generating misleading outputs.

Table 1: Results on POPE [30] benchmark. Higher (\uparrow) accuracy, precision, recall, and F1 indicate better performance. The best results are bolded, and the second-best are underlined.

Setup	Method	LLaVA-1.5			InstructBLIP			Qwen-VL		
		Acc. \uparrow	Prec. \uparrow	F1 \uparrow	Acc. \uparrow	Prec. \uparrow	F1 \uparrow	Acc. \uparrow	Prec. \uparrow	F1 \uparrow
MS-COCO	Regular	83.13	81.94	83.44	83.07	83.02	83.08	87.43	93.56	86.48
	VCD	87.00	86.13	87.15	86.23	88.14	85.88	88.80	93.89	88.11
	M3ID	87.50	87.38	87.52	86.67	88.09	86.41	<u>89.83</u>	95.44	<u>89.17</u>
	RITUAL	88.87	<u>89.23</u>	88.81	88.83	90.48	88.60	89.47	<u>96.32</u>	88.62
	DeGF	<u>89.23</u>	90.17	<u>89.11</u>	<u>89.30</u>	<u>90.68</u>	<u>89.10</u>	89.73	93.19	89.31
	Ours	90.33	89.05	89.38	90.12	91.23	91.38	90.11	96.87	88.92
A-OKVQA	Regular	81.17	78.28	82.08	77.00	73.82	78.44	84.70	88.24	83.96
	VCD	83.10	79.96	83.94	80.07	77.67	80.89	85.13	87.27	84.69
	M3ID	84.30	81.58	84.95	80.97	77.93	81.85	86.27	<u>89.19</u>	<u>85.73</u>
	RITUAL	85.83	84.17	86.17	81.97	78.90	82.87	84.57	84.09	84.67
	DeGF	<u>86.1</u>	<u>84.73</u>	<u>86.37</u>	<u>82.50</u>	<u>79.64</u>	<u>83.31</u>	86.50	86.87	85.71
	Ours	87.67	85.25	88.43	83.52	80.12	83.69	<u>86.34</u>	91.24	86.38
Adversarial	Regular	77.43	73.31	79.26	74.60	71.26	76.45	79.83	80.13	79.73
	VCD	77.17	72.18	79.47	77.20	74.29	78.49	81.33	80.60	81.55
	M3ID	78.23	73.51	80.22	77.47	73.68	79.14	82.03	81.47	82.19
	RITUAL	78.80	74.43	80.54	78.73	74.57	80.39	82.80	83.15	82.71
	DeGF	<u>79.47</u>	<u>75.14</u>	<u>81.09</u>	<u>78.8</u>	78.43	<u>80.11</u>	<u>83.47</u>	<u>84.49</u>	<u>82.98</u>
	Ours	81.67	76.93	82.22	79.61	<u>77.64</u>	79.86	84.36	85.03	83.69
Random	Regular	81.90	76.63	83.53	80.63	76.82	81.92	86.27	90.66	85.48
	VCD	83.83	78.05	85.34	84.20	80.90	85.00	87.87	90.06	87.53
	M3ID	84.67	79.25	85.97	85.43	81.77	86.23	<u>88.13</u>	<u>92.06</u>	87.55
	RITUAL	85.17	79.79	86.40	87.13	83.92	87.71	<u>87.73</u>	92.49	87.01
	DeGF	<u>86.17</u>	<u>80.84</u>	<u>87.27</u>	<u>87.4</u>	<u>84.67</u>	<u>88.02</u>	87.90	89.16	<u>87.58</u>
	Ours	88.67	83.63	89.38	88.94	85.32	89.21	88.33	91.46	88.31
Popular	Regular	75.07	68.58	78.77	75.17	70.15	77.91	84.60	87.99	83.88
	VCD	76.63	69.59	80.19	78.63	73.53	80.72	86.23	87.30	86.03
	M3ID	77.80	70.98	80.91	78.80	73.38	81.00	<u>86.50</u>	89.59	85.95
	RITUAL	78.83	71.99	<u>81.68</u>	78.73	72.83	81.17	<u>86.36</u>	88.73	86.20
	DeGF	<u>79.07</u>	<u>72.11</u>	81.09	<u>80.47</u>	<u>75.61</u>	<u>82.35</u>	86.47	<u>90.74</u>	<u>86.52</u>
	Ours	80.11	72.64	82.36	80.79	76.29	83.76	87.71	90.96	87.26
Adversarial	Regular	67.23	61.56	73.70	69.87	64.54	74.54	76.90	75.59	77.48
	VCD	67.40	61.39	74.21	71.00	65.41	75.45	79.13	76.04	80.30
	M3ID	68.60	62.22	75.11	70.10	64.28	75.16	79.50	77.54	80.21
	RITUAL	68.57	62.26	74.99	70.27	64.15	75.55	80.20	79.08	<u>80.58</u>
	DeGF	<u>70.7</u>	<u>66.7</u>	<u>76.86</u>	<u>71.87</u>	<u>65.65</u>	<u>75.96</u>	<u>80.75</u>	<u>80.37</u>	80.46
	Ours	71.3	68.1	78.26	73.44	66.97	77.16	81.26	80.97	81.04

An important observation is the method's robustness in the more difficult popular and adversarial scenarios. Unlike the random setting, these configurations are characterized by frequent inclusion and co-occurrence of non-existent negative objects [30], which

tend to trigger hallucinations in existing models. Despite this increased complexity, our method experiences significantly smaller drops in performance compared to all other baselines. This suggests that our generative feedback mechanism not only enhances the model's visual grounding but also helps it discern misleading

Table 2: Results on CHAIR [38] benchmark. We limit the maximum number of new tokens to 64. Lower (↓) CHAIR_S , CHAIR_I and higher (↑) recall and length indicate better performance. The best results in each setting are **bolded**, and the second-best are underlined.

Method	LLaVA-1.5				InstructBLIP			
	$\text{CHAIR}_S \downarrow$	$\text{CHAIR}_I \downarrow$	Recall ↑	Length ↑	$\text{CHAIR}_S \downarrow$	$\text{CHAIR}_I \downarrow$	Recall ↑	Length ↑
Regular	26.1	9.3	58.6	53.3	31.3	11.0	59.1	53.5
VCD	24.3	7.8	63.4	<u>54.4</u>	29.9	10.2	61.9	54.1
M3ID	21.5	<u>6.1</u>	64.1	53.6	30.7	10.3	62.5	53.3
RITUAL	22.3	6.8	63.1	54.7	26.7	8.8	63.5	<u>55.2</u>
Woodpecker	24.8	7.6	60.9	49.6	31.1	10.7	62.4	51.4
HALC	21.6	7.2	<u>64.9</u>	53.5	24.6	8.1	<u>64.2</u>	54.8
DeFG	<u>18.4</u>	6.4	62.9	54.3	<u>24.0</u>	<u>7.7</u>	63.5	55.0
Ours	18.1	6.1	65.2	55.7	23.2	7.3	68.9	55.8

Table 3: Results on MME-Hallucination [15] and MMBench [35] benchmark. We present the average MME scores along with their standard deviations over three random seeds for each subset. Additionally, the final column reports the overall accuracy of each method on the MMBench benchmark. Higher values (↑) denote better performance. The best results are highlighted in **bold**, while the second-best are marked with underlining.

Method	Object-level		Attribute-level		MME Score ↑	MMBench ↑
	Existence ↑	Count ↑	Position ↑	Color ↑		
Regular	173.75 (±4.79)	<u>121.67</u> (±12.47)	117.92 (±3.69)	149.17 (±7.51)	562.50 (±3.96)	64.1
DoLa	176.67 (±2.89)	113.33 (±10.41)	90.55 (±8.22)	141.67 (±7.64)	522.22 (±16.78)	63.8
OPERA	183.33 (±6.45)	137.22 (±6.31)	122.78 (±2.55)	155.00 (±5.00)	598.33 (±10.41)	64.4
VCD	186.67 (±5.77)	<u>125.56</u> (±3.47)	128.89 (±6.73)	139.45 (±12.51)	580.56 (±15.13)	64.5
M3ID	186.67 (±5.77)	128.33 (±10.41)	<u>131.63</u> (±5.00)	151.67 (±20.88)	597.50 (±20.35)	64.3
RITUAL	<u>187.53</u> (±2.89)	139.58 (±7.64)	125.00 (±10.27)	<u>163.33</u> (±6.87)	<u>626.29</u> (±20.38)	64.0
Woodpecker	<u>187.53</u> (±2.89)	126.25 (±2.17)	126.66 (±2.89)	149.17 (±17.34)	589.58 (±10.00)	64.2
HALC	183.33 (±0.00)	133.33 (±5.77)	109.58 (±3.69)	155.00 (±5.00)	581.24 (±9.07)	64.4
DeFG	188.33 (±2.89)	<u>142.50</u> (±6.64)	131.33 (±3.85)	163.17 (±3.47)	625.83 (±9.18)	<u>65.2</u>
Ours	190.26 (±2.31)	144.43 (±5.27)	133.71 (±3.14)	165.62 (±4.08)	627.39 (±8.53)	65.9

object associations, thus improving its resistance to context-driven hallucinations.

Results on CHAIR. We evaluate our approach on the open-ended image captioning task and compare it with several state-of-the-art decoding strategies. The CHAIR scores, recall values, and average response lengths are summarized in Table 2. These evaluations are conducted on two representative LVLMs and consistently show that our method outperforms all baselines. Notably, our approach surpasses the second-best method by margins of significant gain on the CHAIR_S metric, respectively. Furthermore, it generates more informative responses than standard decoding, as reflected by its higher recall and longer average output length. These findings highlight the strength of our generative feedback mechanism in enhancing the fidelity and richness of model outputs. By leveraging synthesized visual references during decoding, our method helps the model better ground its predictions in visual content, leading

to a significant reduction in hallucinated objects during caption generation.

Results on MME-Hallucination and MMBench. To evaluate our method beyond object-level hallucinations, we further conduct experiments on the MME-Hallucination benchmark, which covers both object existence and attribute-based hallucination scenarios. As reported in Table 3, our approach consistently surpasses competing baselines, achieving notable improvements in the total score metric, outperforming the second-best method by +18.19 on LLaVA-1.5 and +21.11 on InstructBLIP. Across the eight subcategories, our method secures the highest performance in six, underscoring its robustness across different hallucination types. Notably, our approach yields significant gains on the color subset, which is particularly difficult due to its reliance on accurate interpretation of subtle visual attributes. These findings confirm the strength of our

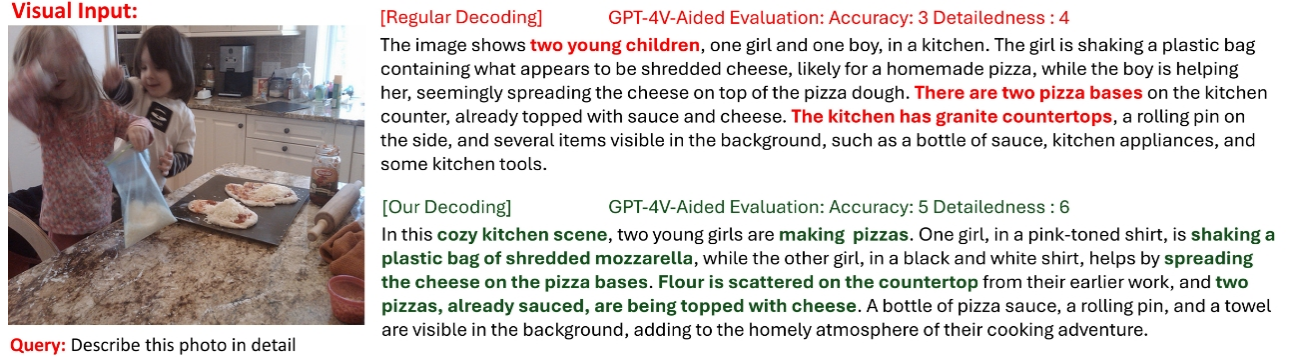


Figure 3: Case study on the LLaVA-Bench benchmark. Responses from standard decoding and our method (LLaVA-1.5) are shown with GPT-4V-assisted evaluations. Hallucinated and correct contents are highlighted in red and green, respectively.

Table 4: Ablation study. We present the performance of our approach on multiple components.

Models	POPE Acc.	CHAIR _S	CHAIR _I	MME Score
Coarse Response(sdv1.5)	89.04	20.3	7.2	626.6
Fine-grained Response(sdv1.5)	89.67	19.8	6.9	634.15
Fine-grained - Coarse Response(sdv1.5)	89.78	18.7	6.3	644.37
Remove Wasserstein Fusion(sdv1.5)	88.01	22.4	6.2	624.29
Coarse Response(sdxl-v1.0)	88.26	19.9	6.7	643.62
Fine-grained Response(sdxl-v1.0)	88.45	19.4	6.4	648.73
Fine-grained - Coarse Response(sdxl-v1.0)	88.60	18.3	5.8	649.38
Remove Wasserstein Fusion(sdxl-v1.0)	87.13	21.8	6.6	638.02
Coarse Response(sd-v2.1)	88.36	20.2	7.3	634.4
Fine-grained Response(sd-v2.1)	88.54	19.25	7.1	644.89
Fine-grained - Coarse Response(sd-v2.1)	88.69	18.44	6.9	647.24
Remove Wasserstein Fusion(sd-v2.1)	87.19	21.3	7.8	631.26

generative feedback mechanism in mitigating both coarse-grained and fine-grained hallucinations.

More details for experiments on other datasets and more case studies can refer to the Appendix.

4.3 Ablation Studies

Study for Components. We conduct an ablation study to evaluate the contributions of coarse-to-fine reasoning and Wasserstein fusion across different diffusion backbones (sdv1.5, sdxl-v1.0, sd-v2.1). As shown in Table 4, results consistently show that combining fine- and coarse-grained responses outperforms using either alone, indicating that multi-level semantic aggregation improves factual grounding and descriptive accuracy. For example, the Fine-grained - Coarse Response setting yields the best CHAIR and MME scores across all backbones, demonstrating reduced hallucinations and enhanced alignment with image content. Removing the Wasserstein fusion module leads to noticeable performance drops, confirming its key role in consolidating diverse semantic cues into a unified and accurate response. The improvements are particularly evident in the CHAIR metrics, highlighting the framework’s robustness in mitigating hallucinated object mentions. Overall, these results validate the effectiveness and generalizability of our proposed fine-to-coarse feedback and fusion strategy.

Effects of Different Generative Models. Table A.3 compares several CoFi-Dec variants that utilize different versions of Stable Diffusion as the generative module, all evaluated using the same LLaVA-1.5 backbone. The results demonstrate that the performance of our method remains stable across different diffusion model choices. Regardless of the specific generative variant, all configurations deliver consistent improvements over the baseline regular decoding. While SD-XL-v1.0 [37] provides marginally better performance, we adopt SD-v1.5 as the default due to its substantially faster image generation time, making it more practical for large-scale or real-time applications.

5 Conclusion

In this work, we present a multi-granularity generative feedback framework to mitigate hallucination in large vision-language models. Inspired by the hierarchical nature of human visual perception, our method integrates the original image with both coarse-grained global context and fine-grained local visual evidence, enabling a structured multi-resolution reasoning process. By leveraging a generative self-verification loop, our approach allows the model to refine its output based on internal visual imagination and cross-granularity consistency. Experimental results demonstrate that our method significantly improves response faithfulness and visual grounding across multiple benchmarks, particularly in scenarios involving ambiguous or detail-intensive visual inputs. Our framework is model-agnostic, modular, and compatible with existing LVLMs, offering a generalizable pathway toward more reliable multimodal generation. Future work includes exploring adaptive granularity selection via tree-structured exploration and incorporating learned feedback quality estimation to further enhance self-correction capabilities.

6 Acknowledgments

This work was supported by the Science and Technology Innovation 2030-Key Project under Grant 2021ZD0201404.

References

- [1] Tomer Amit, Tal Shahrabany, Eliya Nachmani, and Lior Wolf. 2021. Segdiff: Image segmentation with diffusion probabilistic models. *arXiv preprint arXiv:2112.00390* (2021).
- [2] Jinze Bai, Shuai Bai, Shusheng Yang, Shijie Wang, Sinan Tan, Peng Wang, Junyang Lin, Chang Zhou, and Jingren Zhou. 2023. Qwen-vl: A frontier large vision-language model with versatile abilities. *arXiv preprint arXiv:2308.12966* (2023).
- [3] Zechen Bai, Pichao Wang, Tianjun Xiao, Tong He, Zongbo Han, Zheng Zhang, and Mike Zheng Shou. 2024. Hallucination of multimodal large language models: A survey. *arXiv preprint arXiv:2404.18930* (2024).
- [4] Huiwen Chang, Han Zhang, Jarred Barber, Aaron Maschinot, Jose Lezama, Lu Jiang, Ming-Hsuan Yang, Kevin Patrick Murphy, William T Freeman, Michael Rubinstein, et al. 2023. Muse: Text-To-Image Generation via Masked Generative Transformers. In *International Conference on Machine Learning*. PMLR, 4055–4075.
- [5] Beita Chen, Xinyu Lyu, Lianli Gao, Jingkuan Song, and Heng Tao Shen. 2024. Alleviating Hallucinations in Large Vision-Language Models through Hallucination-Induced Optimization. *Advances in Neural Information Processing Systems* (2024).
- [6] Zhaorun Chen, Zhuokai Zhao, Hongyin Luo, Huaxiu Yao, Bo Li, and Jiawei Zhou. 2024. HALC: Object Hallucination Reduction via Adaptive Focal-Contrast Decoding. In *International Conference on Machine Learning*. PMLR, 7824–7846.
- [7] Zhiyang Chen, Yousong Zhu, Yufei Zhan, Zhaowen Li, Chaoyang Zhao, Jinqiao Wang, and Ming Tang. 2023. Mitigating hallucination in visual language models with visual supervision. *arXiv preprint arXiv:2311.16479* (2023).
- [8] Wei-Lin Chiang, Zhuohan Li, Zi Lin, Ying Sheng, Zhanghao Wu, Hao Zhang, Liannmin Zheng, Siyuan Zhuang, Yonghao Zhuang, Joseph E. Gonzalez, Ion Stoica, and Eric P. Xing. 2023. Vicuna: An Open-Source Chatbot Impressing GPT-4 with 90%* ChatGPT Quality. <https://lmsys.org/blog/2023-03-30-vicuna/>
- [9] Aakanksha Chowdhery, Sharan Narang, Jacob Devlin, Maarten Bosma, Gaurav Mishra, Adam Roberts, Paul Barham, Hyung Won Chung, Charles Sutton, Sebastian Gehrmann, et al. 2023. Palm: Scaling language modeling with pathways. *Journal of Machine Learning Research* 24, 1, Article 240 (2023), 113 pages.
- [10] Yung-Sung Chuang, Yujia Xie, Hongyin Luo, Yoon Kim, James R. Glass, and Pengcheng He. 2024. DoLa: Decoding by Contrasting Layers Improves Factuality in Large Language Models. In *International Conference on Learning Representations*. <https://openreview.net/forum?id=Th6NyL07na>
- [11] Florin-Elain Croitoru, Vlad Hondu, Radu Tudor Ionescu, and Mubarak Shah. 2023. Diffusion models in vision: A survey. *IEEE Transactions on Pattern Analysis and Machine Intelligence* 45, 9 (2023), 10850–10869.
- [12] Wenliang Dai, Junnan Li, Dongxu Li, Anthony Tiong, Junqi Zhao, Weisheng Wang, Boyang Li, Pascale Fung, and Steven Hoi. 2023. InstructBLIP: towards general-purpose vision-language models with instruction tuning. *Advances in Neural Information Processing Systems* 36 (2023), 49250–49267.
- [13] Ailin Deng, Zhirui Chen, and Bryan Hooi. 2024. Seeing is believing: Mitigating hallucination in large vision-language models via clip-guided decoding. *arXiv preprint arXiv:2402.15300* (2024).
- [14] Alessandro Favero, Luca Zancato, Matthew Trager, Siddharth Choudhary, Pramuditha Perera, Alessandro Achille, Ashwin Swaminathan, and Stefano Soatto. 2024. Multi-modal hallucination control by visual information grounding. In *Proceedings of the IEEE/CVF Conference on Computer Vision and Pattern Recognition*. 14303–14312.
- [15] Chaoyou Fu, Peixian Chen, Yunhang Shen, Yulei Qin, Mengdan Zhang, Xu Lin, Jinrui Yang, Xiaowu Zheng, Ke Li, Xing Sun, et al. 2023. MME: A Comprehensive Evaluation Benchmark for Multimodal Large Language Models. *arXiv preprint arXiv:2306.13394* (2023).
- [16] Songwei Ge, Taesung Park, Jun-Yan Zhu, and Jia-Bin Huang. 2023. Expressive text-to-image generation with rich text. In *Proceedings of the IEEE/CVF International Conference on Computer Vision*. 7545–7556.
- [17] Ian Goodfellow, Jean Pouget-Abadie, Mehdi Mirza, Bing Xu, David Warde-Farley, Sherjil Ozair, Aaron Courville, and Yoshua Bengio. 2014. Generative adversarial nets. *Advances in Neural Information Processing Systems* 27 (2014).
- [18] Anisha Gunjal, Jihan Yin, and Erhan Bas. 2024. Detecting and preventing hallucinations in large vision language models. In *Proceedings of the AAAI Conference on Artificial Intelligence*, Vol. 38. 18135–18143.
- [19] Jonathan Ho, Ajay Jain, and Pieter Abbeel. 2020. Denoising diffusion probabilistic models. *Advances in Neural Information Processing Systems* 33 (2020), 6840–6851.
- [20] Qidong Huang, Xiaoyi Dong, Pan Zhang, Bin Wang, Conghui He, Jiaqi Wang, Dahua Lin, Weiming Zhang, and Nenghai Yu. 2024. Opera: Alleviating hallucination in multi-modal large language models via over-trust penalty and retrospection-allocation. In *Proceedings of the IEEE/CVF Conference on Computer Vision and Pattern Recognition*. 13418–13427.
- [21] Chaoya Jiang, Haiyang Xu, Mengfan Dong, Jiaxing Chen, Wei Ye, Ming Yan, Qinghao Ye, Ji Zhang, Fei Huang, and Shikun Zhang. 2024. Hallucination augmented contrastive learning for multimodal large language model. In *Proceedings of the IEEE/CVF Conference on Computer Vision and Pattern Recognition*. 27036–27046.
- [22] Qirui Jiao, Daoyuan Chen, Yilun Huang, Yaliang Li, and Ying Shen. 2024. Img-Diff: Contrastive Data Synthesis for Multimodal Large Language Models. *arXiv preprint arXiv:2408.04594* (2024).
- [23] Minguk Kang, Jun-Yan Zhu, Richard Zhang, Jaesik Park, Eli Shechtman, Sylvain Paris, and Taesung Park. 2023. Scaling up gans for text-to-image synthesis. In *Proceedings of the IEEE/CVF Conference on Computer Vision and Pattern Recognition*. 10124–10134.
- [24] Tero Karras, Miika Aittala, Timo Aila, and Samuli Laine. 2022. Elucidating the design space of diffusion-based generative models. *Advances in Neural Information Processing Systems* 35 (2022), 26565–26577.
- [25] Junho Kim, Hyunjun Kim, Yeonju Kim, and Yong Man Ro. 2024. CODE: Contrastive Self-generated Description to Combat Hallucination in Large Multi-modal Models. *Advances in Neural Information Processing Systems* (2024).
- [26] Sicong Leng, Hang Zhang, Guanzheng Chen, Xin Li, Shijian Lu, Chunyan Miao, and Lidong Bing. 2024. Mitigating object hallucinations in large vision-language models through visual contrastive decoding. In *Proceedings of the IEEE/CVF Conference on Computer Vision and Pattern Recognition*. 13872–13882.
- [27] Alexander C Li, Mihir Prabhudesai, Shivam Duggal, Ellis Brown, and Deepak Pathak. 2023. Your diffusion model is secretly a zero-shot classifier. In *Proceedings of the IEEE/CVF International Conference on Computer Vision*. 2206–2217.
- [28] Junnan Li, Dongxu Li, Silvia Savarese, and Steven Hoi. 2023. Blip-2: Bootstrapping language-image pre-training with frozen image encoders and large language models. In *International Conference on Machine Learning*. PMLR, 19730–19742.
- [29] Xiang Lisa Li, Ari Holtzman, Daniel Fried, Percy Liang, Jason Eisner, Tatsunori B Hashimoto, Luke Zettlemoyer, and Mike Lewis. 2023. Contrastive Decoding: Open-ended Text Generation as Optimization. In *Proceedings of the Annual Meeting of the Association for Computational Linguistics*. 12286–12312.
- [30] Yifan Li, Yifan Du, Kun Zhou, Jinpeng Wang, Wayne Xin Zhao, and Ji-Rong Wen. 2023. Evaluating Object Hallucination in Large Vision-Language Models. In *Proceedings of the Conference on Empirical Methods in Natural Language Processing*. 292–305.
- [31] Fuxiao Liu, Kevin Lin, Linjie Li, Jianfeng Wang, Yaser Yacoob, and Lijuan Wang. 2024. Mitigating Hallucination in Large Multi-Modal Models via Robust Instruction Tuning. In *International Conference on Learning Representations*. <https://openreview.net/forum?id=J44Hft14JCg>
- [32] Haotian Liu, Chunyuan Li, Yuheng Li, and Yong Jae Lee. 2024. Improved baselines with visual instruction tuning. In *Proceedings of the IEEE/CVF Conference on Computer Vision and Pattern Recognition*. 26296–26306.
- [33] Haotian Liu, Chunyuan Li, Qingyang Wu, and Yong Jae Lee. 2023. Visual instruction tuning. *Advances in Neural Information Processing Systems* 36 (2023), 34892–34916.
- [34] Hanchao Liu, Wenyuan Xue, Yifei Chen, Dapeng Chen, Xiutian Zhao, Ke Wang, Liping Hou, Rongjun Li, and Wei Peng. 2024. A survey on hallucination in large vision-language models. *arXiv preprint arXiv:2402.00253* (2024).
- [35] Yuan Liu, Haodong Duan, Yuanhan Zhang, Bo Li, Songyang Zhang, Wangbo Zhao, Yike Yuan, Jiaqi Wang, Conghui He, Ziwei Liu, et al. 2024. Mmbench: Is your multi-modal model an all-around player?. In *European Conference on Computer Vision*. Springer, 216–233.
- [36] Alexander Quinn Nichol, Prafulla Dhariwal, Aditya Ramesh, Pranav Shyam, Pamela Mishkin, Bob McGrew, Ilya Sutskever, and Mark Chen. 2022. GLIDE: Towards Photorealistic Image Generation and Editing with Text-Guided Diffusion Models. In *International Conference on Machine Learning*. PMLR, 16784–16804.
- [37] Dustin Podell, Zion English, Kyle Lacey, Andreas Blattmann, Tim Dockhorn, Jonas Müller, Joe Penna, and Robin Rombach. 2024. SDXL: Improving Latent Diffusion Models for High-Resolution Image Synthesis. In *International Conference on Learning Representations*. <https://openreview.net/forum?id=di52zR8xgf>
- [38] Anna Rohrbach, Lisa Anne Hendricks, Kaylee Burns, Trevor Darrell, and Kate Saenko. 2018. Object Hallucination in Image Captioning. In *Proceedings of the Conference on Empirical Methods in Natural Language Processing*. 4035–4045.
- [39] Robin Rombach, Andreas Blattmann, Dominik Lorenz, Patrick Esser, and Björn Ommer. 2022. High-resolution image synthesis with latent diffusion models. In *Proceedings of the IEEE/CVF Conference on Computer Vision and Pattern Recognition*. 10684–10695.
- [40] Chitwan Saharia, William Chan, Saurabh Saxena, Lala Li, Jay Whang, Emily L Denton, Kamyar Ghasemipour, Raphael Gontijo Lopes, Burcu Karagol Ayan, Tim Salimans, et al. 2022. Photorealistic text-to-image diffusion models with deep language understanding. *Advances in Neural Information Processing Systems* 35 (2022), 36479–36494.
- [41] Axel Sauer, Tero Karras, Samuli Laine, Andreas Geiger, and Timo Aila. 2023. Stylegan-t: Unlocking the power of gans for fast large-scale text-to-image synthesis. In *International Conference on Machine Learning*. PMLR, 30105–30118.
- [42] Christoph Schuhmann, Romain Beaumont, Richard Vencu, Cade Gordon, Ross Wightman, Mehdi Cherti, Theo Coombes, Aarush Katta, Clayton Mullis, Mitchell Wortsman, et al. 2022. Laion-5b: An open large-scale dataset for training next generation image-text models. *Advances in Neural Information Processing Systems* 35 (2022), 25278–25294.
- [43] Zhiqing Sun, Sheng Shen, Shengcao Cao, Haotian Liu, Chunyuan Li, Yikang Shen, Chuang Gan, Liang-Yan Gui, Yu-Xiong Wang, Yiming Yang, et al. 2023. Aligning large multimodal models with factually augmented rlhf. *arXiv preprint arXiv:2309.14525* (2023).

[44] Shengbang Tong, Zhuang Liu, Yuexiang Zhai, Yi Ma, Yann LeCun, and Saining Xie. 2024. Eyes wide shut? exploring the visual shortcomings of multimodal llms. In *Proceedings of the IEEE/CVF Conference on Computer Vision and Pattern Recognition*. 9568–9578.

[45] Hugo Touvron, Thibaut Lavril, Gautier Izacard, Xavier Martinet, Marie-Anne Lachaux, Timothée Lacroix, Baptiste Rozière, Naman Goyal, Eric Hambro, Faisal Azhar et al. 2023. Llmas: Open and efficient foundation language models. *arXiv preprint arXiv:2302.13971* (2023).

[46] Xintong Wang, Jingheng Pan, Liang Ding, and Chris Biemann. 2024. Mitigating hallucinations in large vision-language models with instruction contrastive decoding. In *Findings of the Association for Computational Linguistics ACL 2024*. 15840–15853.

[47] Julia Wolleb, Robin Sandkühler, Florentin Bieder, Philippe Valmaggia, and Philippe C Cattin. 2022. Diffusion models for implicit image segmentation ensembles. In *International Conference on Medical Imaging with Deep Learning*. PMLR, 1336–1348.

[48] Sangmin Woo, Jaehyuk Jang, Donguk Kim, Yubin Choi, and Changick Kim. 2024. RITUAL: Random Image Transformations as a Universal Anti-hallucination Lever in LVLMs. *arXiv preprint arXiv:2405.17821* (2024).

[49] Mingrui Wu, Jiayi Ji, Oucheng Huang, Jiale Li, Yuhang Wu, Xiaoshuai Sun, and Rongrong Ji. 2024. Evaluating and Analyzing Relationship Hallucinations in LVLMs. In *International Conference on Machine Learning*. PMLR, 53553–53570.

[50] Ling Yang, Zhilong Zhang, Yang Song, Shenda Hong, Runsheng Xu, Yue Zhao, Wentao Zhang, Bin Cui, and Ming-Hsuan Yang. 2023. Diffusion models: A comprehensive survey of methods and applications. *Comput. Surveys* 56, 4 (2023), 1–39.

[51] Qinghao Ye, Haiyang Xu, Jiabo Ye, Ming Yan, Anwen Hu, Haowei Liu, Qi Qian, Ji Zhang, and Fei Huang. 2024. mplug-owl2: Revolutionizing multi-modal large language model with modality collaboration. In *Proceedings of the IEEE/CVF Conference on Computer Vision and Pattern Recognition*. 13040–13051.

[52] Shukang Yin, Chaoyou Fu, Sirui Zhao, Tong Xu, Hao Wang, Dianbo Sui, Yunhang Shen, Ke Li, Xing Sun, and Enhong Chen. 2023. Woodpecker: Hallucination correction for multimodal large language models. *arXiv preprint arXiv:2310.16045* (2023).

[53] Jiahui Yu, Yuanzhong Xu, Jing Yu Koh, Thang Luong, Gunjan Baid, Zirui Wang, Vijay Vasudevan, Alexander Ku, Yinfei Yang, Burcu Karagol Ayan, Ben Hutchinson, Wei Han, Zarana Parekh, Xin Li, Han Zhang, Jason Baldridge, and Yonghui Wu. 2022. Scaling Autoregressive Models for Content-Rich Text-to-Image Generation. *Transactions on Machine Learning Research* (2022). <https://openreview.net/forum?id=AFDcYJKhND>

[54] Zihao Yue, Liang Zhang, and Qin Jin. 2024. Less is More: Mitigating Multimodal Hallucination from an EOS Decision Perspective. In *Proceedings of the Annual Meeting of the Association for Computational Linguistics*. 11766–11781.

[55] Fangneng Zhan, Yingchen Yu, Rongliang Wu, Jiahui Zhang, Shijian Lu, Lingjue Liu, Adam Kortylewski, Christian Theobalt, and Eric Xing. 2023. Multimodal image synthesis and editing: A survey and taxonomy. *IEEE Transactions on Pattern Analysis and Machine Intelligence* 45, 12 (2023), 15098–15119.

[56] Ce Zhang, Zifu Wan, Zhehan Kan, Martin Q Ma, Simon Stepputtis, Deva Ramanan, Russ Salakhutdinov, Louis-Philippe Morency, Katia Sycara, and Yaqi Xie. 2025. Self-Correcting Decoding with Generative Feedback for Mitigating Hallucinations in Large Vision-Language Models. *ICLR* (2025).

[57] Jinrui Zhang, Teng Wang, Haigang Zhang, Ping Lu, and Feng Zheng. 2024. Reflective Instruction Tuning: Mitigating Hallucinations in Large Vision-Language Models. In *European Conference on Computer Vision*. https://www.ecva.net/papers/eccv_2024/papers_ECCV/papers/08550.pdf

[58] Xinran Zhao, Hongming Zhang, Xiaoman Pan, Wenlin Yao, Dong Yu, Tongshuang Wu, and Jianshu Chen. 2024. Fact-and-Reflection (FaR) Improves Confidence Calibration of Large Language Models. In *Findings of the Association for Computational Linguistics ACL 2024*. 8702–8718.

[59] Yiyang Zhou, Chenhang Cui, Jaehong Yoon, Linjun Zhang, Zhen Deng, Chelsea Finn, Mohit Bansal, and Huaxiu Yao. 2024. Analyzing and Mitigating Object Hallucination in Large Vision-Language Models. In *International Conference on Learning Representations*. <https://openreview.net/forum?id=oZDJKTlOUe>

[60] Minfeng Zhu, Pingbo Pan, Wei Chen, and Yi Yang. 2019. Dm-gan: Dynamis memory generative adversarial networks for text-to-image synthesis. In *Proceedings of the IEEE/CVF Conference on Computer Vision and Pattern Recognition*. 5802–5810.

Table A2: Efficiency comparison. For each method, we present the average inference latency per instance and peak GPU memory. Experiments are conducted on a single RTX A6000 Ada GPU.

Method	Avg. Latency ↓	GPU Memory ↓	CHAIR _S ↓
Regular	3.44 s (x1.00)	15778 MB (x1.00)	55.0
VCD	6.91 s (x2.01)	16634 MB (x1.05)	54.4
OPERA	24.70 s (x7.18)	22706 MB (x1.44)	52.6
Woodpecker	10.68 s (x3.10)	22199 MB (x1.41)	57.6
HALC	22.61 s (x6.51)	23084 MB (x1.46)	51.0
DeFG	13.89 s (x4.04)	19119 MB (x1.21)	48.8
Ours	20.83 s (x6.05)	18597 MB (x1.28)	46.7

Table A3: Effects of different generative models. We report the performance of different variants of our method, utilizing various stable diffusion models, on the LLaVA-1.5 backbone.

Models	POPE Acc.	CHAIR _S	CHAIR _I	MME Score
Regular	83.13	26.2	9.4	562.50
SD-v1.1	88.37	19.3	6.5	638.33
SD-v1.5	89.03	18.4	6.1	644.44
SD-v2.1	88.70	18.8	6.7	632.22
SD-XL-v0.9	88.87	18.6	6.1	642.50
SD-XL-v1.0	88.60	17.9	5.8	648.33

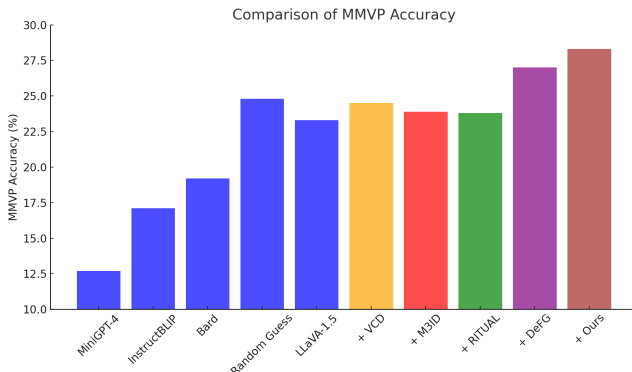


Figure 1: Results on MMVP [44]. We apply our approach to LLaVA-1.5 [32] and compare its performance against other hallucination mitigation methods.

Table A1: GPT-4V-aided evaluation on LLaVA-Bench

. Higher accuracy and detailedness (↑) indicate better performance. The evaluation is performed on LLaVA-1.5 [32].

Method	LLaVA-1.5		InstructBLIP	
	Acc. ↑	Det. ↑	Acc. ↑	Det. ↑
Regular	2.88	3.29	3.42	3.96
DeFG	4.29	4.54	4.38	4.79
Ours	4.33	4.57	4.33	4.86
VCD	3.62	3.83	3.71	4.21
DeFG	4.04	4.38	4.17	4.58
Ours	4.12	4.31	4.26	4.63
M3ID	3.88	4.08	4.00	4.33
DeFG	4.04	4.29	4.08	4.50
Ours	4.13	4.18	4.27	4.51

A More Experimental Results and Analysis

Results on MMVP. To further evaluate the model’s ability in fine-grained visual discrimination, we run experiments on the MMVP benchmark. As illustrated in Figure 1, applying our self-refining decoding technique to LLaVA-1.5 elevates performance from 22.67% to 27.33%. Compared to other hallucination mitigation baselines, our method yields more substantial improvements, particularly in tasks that require distinguishing visually similar images with subtle differences. These results highlight our approach’s ability to improve precision in visual recognition by reducing misinterpretations and hallucinated features, thus delivering more accurate outputs in nuanced visual tasks.

Results on LLaVA-Bench. Figure 3 showcases a qualitative comparison using LLaVA-Bench, where we examine the responses generated by standard decoding and our CoFi-Dec-enhanced decoding with LLaVA-1.5. Regular decoding often produces vague or hallucinated descriptions, such as references to “the island below the mountain” or general observations like “cloudy sky” and “cohesive landscape”, which lack specificity. In contrast, our method produces more grounded and informative outputs, accurately identifying elements such as the volcano, the road, nearby vegetation, and residential areas. GPT-4V-assisted evaluation results, summarized in Table A1, further validate these observations, showing that our method outperforms baselines like VCD and M3ID in both response accuracy and descriptive detail.

Efficiency Comparison. In Table A2, we present a comparative analysis of the computational efficiency of our method versus other baseline approaches on the CHAIR benchmark, utilizing the LLaVA-1.5 model with a maximum sequence length of 128 tokens. Our method requires two forward passes and integrates a text-to-image generation step to suppress hallucinations, which leads to a latency increase of approximately 4.04× and a GPU memory overhead of 1.21× relative to standard decoding. The full inference process in our framework consists of three sequential phases: (1) initial response generation, (2) visual feedback generation via a diffusion model, and (3) refinement of the original response. On average, these stages take 3.4s, 3.8s, and 6.6s per sample, respectively. Although our method is less efficient than simpler techniques like standard or contrastive decoding, it is notably more efficient than computationally intensive approaches such as OPERA and HALC. Importantly, our framework consistently achieves the lowest hallucination rates across all evaluated methods.

Table A4: Another results on POPE [30] benchmark. Higher (\uparrow) accuracy, precision, recall, and F1 indicate better performance. The best results are **bolded, and the second-best are underlined.**

Setup	Method	LLaVA-1.5			InstructBLIP			Qwen-VL		
		Acc. \uparrow	Prec. \uparrow	F1 \uparrow	Acc. \uparrow	Prec. \uparrow	F1 \uparrow	Acc. \uparrow	Prec. \uparrow	F1 \uparrow
GQA	Regular	82.23	76.32	84.03	79.67	76.05	80.99	84.90	89.51	83.96
	VCD	83.23	76.73	85.05	82.83	80.16	83.56	85.21	92.05	84.21
	M3ID	84.20	78.00	85.77	83.07	80.06	83.87	85.69	93.11	84.67
	RITUAL	86.10	80.30	87.31	84.87	82.52	<u>85.39</u>	<u>86.1</u>	93.78	84.81
	DeGF	<u>87.09</u>	<u>80.46</u>	<u>87.96</u>	<u>85.40</u>	<u>85.64</u>	85.12	85.95	<u>94.22</u>	<u>85.08</u>
	Ours	89.03	81.1	89.06	86.78	87.06	86.39	87.14	94.65	86.32
Popular	Regular	73.47	66.83	77.84	73.33	68.72	76.26	81.33	83.38	80.74
	VCD	72.37	65.27	77.58	<u>76.13</u>	71.10	78.68	81.97	82.82	81.73
	M3ID	73.87	66.70	78.49	75.17	69.94	78.04	82.13	84.58	81.48
	RITUAL	74.80	67.50	79.15	74.50	69.17	77.61	81.13	85.48	81.03
	DeGF	<u>75.12</u>	<u>71.56</u>	<u>80.98</u>	75.34	<u>71.89</u>	77.96	<u>82.10</u>	<u>86.39</u>	<u>81.85</u>
	Ours	78.56	73.28	83.34	76.18	73.17	<u>78.65</u>	83.54	87.24	83.09
Adversarial	Regular	68.60	62.43	74.84	68.60	63.94	73.10	79.03	80.43	78.54
	VCD	68.83	62.26	75.43	71.00	65.75	75.14	80.87	81.07	80.80
	M3ID	68.67	62.16	75.28	71.17	65.79	<u>75.36</u>	81.03	82.93	<u>80.94</u>
	RITUAL	68.23	61.75	75.10	70.17	64.76	74.78	81.07	83.29	80.41
	DeGF	<u>74.07</u>	<u>67.42</u>	<u>78.22</u>	<u>72.45</u>	<u>68.52</u>	75.32	<u>81.13</u>	<u>84.18</u>	80.57
	Ours	75.21	68.34	79.76	73.25	69.68	76.87	81.69	84.96	81.67

Visual Input:



Query: Describe this photo in detail.

[Regular Decoding]

GPT-4V-Aided Evaluation: Accuracy:3 Detailedness:4

This image shows a modern **office space** with a large **wooden desk** in the center. The room features a fancy **silver chandelier** with **blue crystals** hanging from the ceiling. On the left side, there's a bookshelf containing several **laptops** and **office supplies**. The **marble countertop** houses a **microwave** and a small **coffee machine**. There's a vase with **yellow roses** visible in the corner. The wall has a large **television screen** mounted next to a **bathroom mirror**. The color scheme is dominated by **dark brown** and **gray tones**, giving it a corporate atmosphere.

[Our Approach]

GPT-4V-Aided Evaluation: Accuracy:7 Detailedness:6

This image shows a charming rustic **kitchen** with shabby chic design elements. The room features an elegant **crystal chandelier** with hanging **crystal pendants** above. There's an **open shelving unit** on the left wall displaying colorful **glassware** and **dishware**. The **farmhouse sink** with a traditional **faucet** is installed in a **white brick-faced cabinet base**. A beautiful **ornate gold-framed mirror** hangs on the wall, reflecting the chandelier. There's a small **blue screen** near the sink. On the left side is a vase with **vibrant orange tulips**. The overall color palette is warm with **cream walls** creating a cozy, elegant atmosphere.

Figure A2: Case study on the LLaVA-Bench benchmark. We compare the responses generated by regular decoding and our method using LLaVA-1.5. GPT-4V-aided evaluation results are also provided alongside the responses. Hallucinated and accurate content is highlighted in red and green.

Visual Input:**Query:** Describe this photo in detail.**[Regular Decoding]****GPT-4V-Aided Evaluation: Accuracy:3 Detailedness:4**

The image shows a **tennis match** taking place on a **clay court**. A player wearing a **yellow jersey with number 86** is about to hit a **basketball** with his foot. Several **adult athletes** are scattered across the **indoor gymnasium**. There's a **volleyball net** visible on the right side, and some **spectators** are sitting on **benches** in the background. The **professional athlete** appears to be wearing **red cleats** and the sky has a **stormy appearance** with **dark clouds**.

[Our Approach]**GPT-4V-Aided Evaluation: Accuracy:7 Detailedness:6**

The image shows a **youth soccer game** taking place on a **grassy field**. A player wearing a **blue jersey with number 46** is about to kick a **soccer ball** in mid-air. Several other **young players** in **blue and white uniforms** are positioned across the **outdoor field**. There's a **soccer goal** visible on the right side, and some **residential houses** can be seen in the background. The sky has a **clear blue appearance** with some **white clouds**, indicating it's a **sunny day**.

Figure A3: Case study on the LLaVA-Bench benchmark.**Visual Input:****Query:** Describe this photo in detail.**[Regular Decoding]****GPT-4V-Aided Evaluation: Accuracy:3 Detailedness:4**

The image shows a person **snowboarding down a mountain path**. They are wearing a **blue jacket** with a competition number and a **colorful hat**. The individual is using **wooden snowshoes** to navigate through the **heavy rainfall** on the slope. In the background, there are **palm trees** lining the path. The **male competitor** appears to be participating in some kind of winter **obstacle course** as indicated by the **red flag markers** on the ground. The conditions seem **sunny and clear** despite the winter setting.

[Our Approach]**GPT-4V-Aided Evaluation: Accuracy:7 Detailedness:6**

The image shows a **cross-country skier** moving along a **snow-covered trail**. The person is wearing a **black top** with a competition bib number, **red and white pants**, and a **patterned headband**. They are using **cross-country ski poles** and **skis** to propel themselves across the snowy terrain. The trail is surrounded by **evergreen trees** in a forest setting. The weather appears to be overcast or snowy with some precipitation visible in the image. The skier is in an athletic position, demonstrating proper Nordic skiing technique as they navigate the **groomed trail**. This appears to be part of a **winter skiing competition** based on the numbered bib the athlete is wearing.

Figure A4: Case study on the LLaVA-Bench benchmark.**Visual Input:****Query:** Describe this photo in detail.**[Regular Decoding]****GPT-4V-Aided Evaluation: Accuracy:3 Detailedness:4**

This tranquil scene shows a wide **desert landscape** with a small puddle in the center. Several **flamingos** are wading through the shallow water. The background features a line of **palm trees** creating shade on a hot day. The foreground is dominated by **tall wheat fields** ready for harvest. The **red sunset** in the sky creates a dramatic backdrop against the otherwise peaceful scene.

[Our Approach]**GPT-4V-Aided Evaluation: Accuracy:7 Detailedness:6**

This serene landscape shows a calm **body of water** (likely a lake or river) with a natural shoreline. The foreground features **tall grass** or reeds growing along the water's edge. The background shows a dense line of **green trees** creating a natural border around the water. The **sky** is partly cloudy with soft white clouds against a blue backdrop. The overall scene captures a peaceful natural wetland environment with no people or structures visible, emphasizing the undisturbed natural setting.

Figure A5: Case study on the LLaVA-Bench benchmark.

Visual Input:**Query:** Describe this photo in detail.**[Regular Decoding]****GPT-4V-Aided Evaluation: Accuracy:3 Detailedness:4**

The image shows several slices of **chocolate cake** arranged on a wooden serving platter. A large **meat cleaver** with a black handle lies next to the dessert, ready to serve more portions. The **dark brown frosting** on the cake looks rich and decadent. In the background, there appears to be a **glass of milk** partially visible, perfect for accompanying this sweet treat. The **marble countertop** provides an elegant surface for this appetizing display.

[Our Approach]**GPT-4V-Aided Evaluation: Accuracy:7 Detailedness:6**

The image shows slices of **artisanal bread** with a golden-brown crust arranged on a wooden **cutting board**. A **serrated bread knife** with a white blade and black handle is positioned at the bottom of the frame. The bread appears to be freshly baked, with a dusting of flour still visible on the crust. The natural **wooden surface** beneath enhances the rustic, homemade quality of the scene. The close-up perspective highlights the texture of both the bread and the knife's serrated edge, suggesting preparation for a meal.

Figure A6: Case study on the LLaVA-Bench benchmark.**Visual Input:****Query:** Describe this photo in detail.**[Regular Decoding]****GPT-4V-Aided Evaluation: Accuracy:3 Detailedness:4**

This image shows a **yellow Labrador puppy** lying on a patterned rug. Next to the dog is a **wine bottle** with a red label. The pet appears to be sleeping in what looks like a **kitchen area** with **tile flooring**. There's a **leather couch** partially visible in the background. The lighting suggests it's a **bright afternoon** scene with sunlight streaming through nearby windows. The dog's **collar** has a large tag visible.

[Our Approach]**GPT-4V-Aided Evaluation: Accuracy:7 Detailedness:6**

The image shows an **orange tabby cat** with long fur resting on a **multicolored plaid blanket** or cushion. Next to the cat is a bottle of **Don Julio tequila** with its distinctive round shape and cream-colored cap. The cat appears to be in a relaxed state with eyes partly closed. The setting seems to be indoors on a **carpeted floor**, possibly near a fireplace or alcove with **white walls** visible in the background. The cat has a **fluffy appearance** and seems comfortable in this cozy corner with the random placement of the alcohol bottle creating an unusual juxtaposition.

Figure A7: Case study on the LLaVA-Bench benchmark.**Visual Input:****Query:** Describe this photo in detail.**[Regular Decoding]****GPT-4V-Aided Evaluation: Accuracy:3 Detailedness:4**

The image shows a person's hand reaching into a **pizza box** containing several **cupcakes**. The person is using a **fork** to cut into one of the desserts. There are four **chocolate cookies** arranged neatly in the white container. The **top cookie** has some **yellow sprinkles** on it while the others have white icing drizzled on top with small **cherry pieces** in the center. The **paper plates** under each item help keep the box clean. The background appears to be a **wooden table** with a **blue tablecloth**.

[Our Approach]**GPT-4V-Aided Evaluation: Accuracy:7 Detailedness:6**

The image shows a person's hand reaching into a **white box** containing four **donuts**. The person is using a **wooden stick** to cut or pick at one of the donuts. The box contains various types of **glazed donuts** - one with **yellow crumbs** on top of white cream, and three with **chocolate glaze** and white icing drizzled on top. One donut has what appears to be a **small dough ball** in the center. The donuts are arranged in the box which sits on what seems to be a **light blue surface**. The person's hand is coming from the left side of the image, manipulating one of the chocolate-glazed donuts.

Figure A8: Case study on the LLaVA-Bench benchmark.

Visual Input:**[Regular Decoding]****GPT-4V-Aided Evaluation: Accuracy:3 Detailedness:4**

The image shows a busy **farmer's market** with several people gathered around various **food stalls**. In the foreground, three men are examining a **vintage car** with a red hood. One man is wearing a **Triumph** t-shirt while talking to two others wearing **police uniforms**. Behind them are rows of **bicycles** for rent and a **fruit vendor** with colorful produce. The background features several **wooden shacks** and a **church tower** visible in the distance. The scene looks like a **weekend festival** with families enjoying their time shopping for **local crafts** and food.

Query: Describe this photo in detail.**[Our Approach]****GPT-4V-Aided Evaluation: Accuracy:7 Detailedness:6**

The image shows a **motorcycle gathering** or meetup in what appears to be an urban area. In the foreground, three men are conversing near several parked **motorcycles**. One man is wearing a white **Triumph Motorcycles** t-shirt, while the other two are dressed in **black leather jackets** typical of motorcycle riders, with one wearing a **helmet**. Behind them is a large collection of parked **motorcycles** and many other **motorcycle enthusiasts** in the background. The setting includes **cobblestone pavement** in the foreground and **apartment buildings** visible in the background. The scene captures the **social atmosphere** of a motorcycle club meeting or rally with **clear sunny weather**.

Figure A9: Case study on the LLaVA-Bench benchmark.